A Space-Time PGD-DIC Algorithm

Jean-Charles Passieux, Robin Bouclier, Jean-Noël Périé

Noname manuscript No.
(will be inserted by the editor)

A space-time PGD-DIC algorithm:
Application to 3D mode shapes measurements

J.-C. Passieux, R. Bouclier, J.N. Périé

Received: date / Accepted: date

Abstract The aim of this study is to develop a new regularized Digital Image Correlation (DIC) method for time dependent measurements. The correlation problem is written as a minimization problem over the space-time domain in a general formulation including 2D-DIC and Stereo DIC (SDIC). The unknown time-resolved displacement field is found as a sum of products of space and time functions, similarly to the Proper Generalized Decomposition in computational mechanics. It is shown that the space fields are less sensitive to noise as time regularity acts as a physical regularization of the space fields. The proposed method is illustrated by vibration measurement under harmonic excitation in 2D-DIC and SDIC.

Keywords digital image correlation, proper generalized decomposition, vibrations, dynamics

1 Introduction

Dynamic tests are often instrumented by accelerometers, strain gauges or laser vibrometers because of their excellent measurement resolution. However, in a context of validation and dialogue with simulations, these tools provide a relatively small number of point data compared to the abundance of data resulting from finite element simulations. The number of accelerometers or strain gauges that can be placed on a structure is very limited, on the one hand, because of the cost (in terms of both the equipment itself andthe manpower for setting it up) and on the other hand because of the mass loading and/or mass damping effects which may significantly modify the dynamics of lightweight structures. Finally, the position of these sensors must be carefully chosen to avoid mode shape nodes.

Although Scanning Laser Doppler Vibrometers (SLDV) are contactless (i.e. do not add mass), they usually do not acquire all the measuring points simultaneously. In addition requiring stationarity assumption (assuming no thermal effects, no fatigue and no mode switching), this technical limitation reduces the number of

J.-C. Passieux
Université de Toulouse, Institut Clément Ader (ICA); INSA-UT3-ISAE-Mines Albi-CNRS
E-mail: passieux@insa-toulouse.fr

measurement points available in practice as reasonable acquisition times need to be preserved. It is worth noting that 3D SLDV combining three laser scan heads can estimate complex mode shapes exhibiting three-dimensional displacements. However, this technique remains relatively expensive and is sensitive to large rigid body motion of the specimen[18]. For these reasons, SLDV is mostly used in 1D to measure out-of-plane velocities.

Since the late 2000s, and thanks to the development of high-speed cameras, the instrumentation of vibration tests based on Digital Image Correlation (DIC) is becoming an increasingly credible technique, since (a) it is contact-less (no modification of the dynamics of the structure being analysed), (b) it provides several orders of magnitude more data points than can be obtained with lasers, (c) it handles all the measurement points simultaneously, (d) it is robust with respect to large displacements and to a large frequency range and (e) 3D displacement fields can be measured when Stereo Digital Image Correlation (SDIC) is used. The disadvantage is that the measurement resolution is, in general, not comparable with that of the tools mentioned above [18,5,32]. Special attention must therefore be paid to reducing measurement uncertainties when attempting to develop a new DIC method in this context.

Specifically, the authors generally use SDIC with high-speed cameras to analyze dynamic tests with a harmonic excitation [34,38,15], a shock [34,18] or a random excitation [34,18,39,5,32]. From full field displacement measurements, different mode shapes are extracted by using *e.g.* Fourier analysis and modal curve fitting [34,32] or using lock-in amplifiers [15] in a post-processing phase. In [38], the authors use an *a posteriori* sinusoidal fitting method to increase the accuracy of the displacement measurement of fatigue crack growth tests.

The above literature on the use of DIC as a means of measurement in the vibratory domain essentially consists of two steps that extract modal information from images (raw data). First, a conventional DIC measurement is performed, then the displacement fields (derived from the DIC software) are post-processed using a modal identification procedure. The disadvantage of this two-step approach is that the uncertainties of DIC measurements may propagate in the post-processing. In the case of a harmonic excitation, we show that if the two steps are integrated, *i.e.* if the harmonicity of the displacement field is directly exploited in the image correlation algorithm, then the uncertainty can be greatly reduced, compared to the approach of [38].

In addition, the extra projection steps necessary to compare a Finite Element (FE) model and the data measured by a conventional DIC package (in the form of a point cloud) are sources of further uncertainties. For instance, [39] proposes to use shape features to bridge efficiently the large DIC data sets to the FE model. Here, we propose to use a Finite Element based Digital Image Correlation (FE-DIC) method. The recent developments in the field of FE-DIC [35,7] and the even more recent advances in Finite Element Stereo DIC (FE-SDIC) [13,29,28,33] allow a direct link with the simulation tools. It is thus possible to share the same FE mesh during the calculation and the measurement, in the aim of (a) greatly simplifying the bridge between simulation and experimentation, and (b) limiting the uncertainties associated with reprojection.

In the field of time-dependent problems, Digital Image Correlation generally uses camcorders or high speed digital cameras that can provide a series of images: one (pair of) image(s) for each time step according to the chosen acquisition

framerate. This yields a large amount of data that is usually analysed incrementally, in other words each image pair is analysed independently. Having a temporal resolution much lower than the characteristic time of the observed mechanical phenomena does not really improve measurement uncertainties, even if, at this scale, the evolution of the displacements is smooth. In this paper we propose to prescribe time-smoothness as a physical regularization technique in the space domain. This technique should not be opposed to existing space regularization methods [20,30, 31,28,11,33], but should be rather seen as an additional tool, which can positively complement more conventional remedies. More precisely, the method starts from a space-time formulation of DIC [6,8]. Then the displacement is calculated as a sum of products of separated space and time functions over the full time interval. This can be seen as an extension of the Proper Generalized Decomposition (PGD) method previously proposed in DIC [27] and Digital Volume Correlation (DVC) [17] where the dimensions of space are separated in the same way. It is worth noting that the proposed PGD-DIC method is not limited to global DIC and could also be applied to sub-set based approaches. The method is particularized in this paper to the case of linear vibrations where the time function is harmonic. The method is presented in a general formalism that includes DIC and SDIC. Its ability to reduce noise sensitivity is illustrated on both 2D and Stereo DIC analysis of vibration tests.

The main disadvantage of the approach is that it requires the implementation of a particular DIC algorithm. However, it is shown that the space-time formulation is non-intrusive, so, starting from a classic global DIC code, the extra implementation effort is very small here.

Eventually, as initially proposed in [38,40], this method can still be used with low speed equipments, which has the great advantage to lighten the effects of the trade-off between frame rate and image definition.

2 Incremental approach

The analysis of a time series of images corresponding to an evolution problem is generally performed by analysing each image pair independently. In this section, particular care is taken to provide a global formalism that is suitable for both standard Finite Element Digital Image Correlation (FE-DIC [35,7]) and the newly developed Finite Element Stereo Digital Image Correlation (FE-SDIC [13,28,33]).

Let Ω_s be a space domain, referred to as the Region Of Interest (ROI) and defined such that $\Omega_s \subset \mathbf{R}^2$ is a plane surface in DIC and $\Omega_s \subset \mathbf{R}^3$ denotes, in SDIC, the visible surface of a 3D specimen that is not necessarily planar. We emphasize that, as opposed to classic formulations of DIC, where Ω_s is a subset of an image (see subset methods [21,37]), here, Ω_s is a physical domain expressed in the coordinate system of the specimen. This ROI is observed by n_c digital cameras producing an n_c-uplet of space-time images $\mathcal{I}^c(\mathbf{y},t)$ defined for any point $\mathbf{y} \in \mathbf{R}^2$ in the image coordinate system, for any time t and any camera $c \in \{1,...,n_c\}$. Given Ω_s and a time interval $\Omega_t = [t_0, t_f]$, the unknown displacement $\mathbf{u}(\mathbf{x},t)$ is sought to verify the grey level conservation over the space-time domain $\Omega_s \times \Omega_t$

on each camera as follows:

$$\text{Find } \mathbf{u}(\mathbf{x},t) \text{ such that } \quad r^c(\mathbf{u}(\mathbf{x},t),\mathbf{x},t)=0, \quad \forall \mathbf{x}\in\Omega_s, \quad \forall t\in\Omega_t, \quad \forall c\in\{1,...,n_c\} \tag{1}$$

where the space-time grey level residual is defined by

$$r^c(\mathbf{u}(\mathbf{x},t),\mathbf{x},t)=\mathcal{I}^c(\mathbf{p}^c(\mathbf{x}+\mathbf{u}(\mathbf{x},t)),t)-\mathcal{I}^c(\mathbf{p}^c(\mathbf{x}),t_0) \tag{2}$$

Operator $\mathbf{p}^c$ is the projective model of camera c that maps a point $\mathbf{x}$ of Ω_s in the specimen reference system to the corresponding 2D point $\mathbf{y}=\mathbf{p}^c(\mathbf{x})$ in the image plane of $\mathcal{I}^c$. These models depend on a set of intrinsic (focal length, distortions, etc.) and extrinsic (position/orientation of the camera with respect to the specimen) parameters that must be identified in a calibration phase (see [16][36][29]).

Remark:

- When using a single front parallel camera ($n_c=1$) and a planar test, the method turns into a generalization of the 2D-**DIC** method that has the advantage of accounting for distortions natively when using non-linear camera models [29]. $\mathbf{u}$ denotes a two-component displacement field. It is also possible to use a degraded pinhole model such as:

$$\mathbf{y}=\mathbf{p}^c(\mathbf{x})=\begin{pmatrix} N_f-k\,\mathbf{x}_2 \\ \mathbf{x}_1 \end{pmatrix}$$

  where N_f denotes the number of pixels of the image in the vertical direction and the scale factor k is introduced as the number of pixels per unit length. In this case, the method corresponds exactly to a classic FE-DIC approach, except that $\mathbf{u}$ is directly expressed in the specimen units (*e.g.*, millimetres) and in the specimen's system.
- **SDIC** allows the three components of the displacement in Ω_s to be measured when using a larger number of inclined cameras $n_c>1$. In this case, $\mathbf{u}$ denotes a three-component displacement field [28].

The time domain is naturally discretized in the sense that space-time image $\mathcal{I}^c(\mathbf{y},t)$ is, in practice, represented by a set of n_t+1 static images $\mathcal{I}^c_k(\mathbf{y})=\mathcal{I}^c(\mathbf{y},t_k)$ (including the reference image $\mathcal{I}^c_0(\mathbf{y})$). In a classic approach, each image is analysed sequentially, namely, the displacement $\mathbf{u}_k(\mathbf{x})=\mathbf{u}(\mathbf{x},t_k)$ at the k^{th} time-step is sought to match image $\mathcal{I}^c_k$ to reference image $\mathcal{I}^c_0$. In the following, the dependence on $\mathbf{x}$ of the displacement field $\mathbf{u}_k$ will be omitted for clarity. Problem (1) becomes in its incremental form:

$$\text{Find } \mathbf{u}_k \text{ such that: } \quad r^c_k(\mathbf{u}_k,\mathbf{x})=0, \quad \forall \mathbf{x}\in\Omega_s, \quad \forall k\in\{1,..,n_t\} \quad \forall c\in\{1,...,n_c\} \tag{3}$$

where $r^c_k(\mathbf{u}_k,\mathbf{x})=\mathcal{I}^c_k(\mathbf{p}^c(\mathbf{x}+\mathbf{u}_k))-\mathcal{I}^c_0(\mathbf{p}^c(\mathbf{x}))$ constitutes the grey level residual map associated with the registration of images $\mathcal{I}^c_0$ and $\mathcal{I}^c_k$ using displacement field $\mathbf{u}_k$.

Problem (3) being ill-posed, it is classically written as a set of n_t independent least-square problems (one for each time step k) over the space domain only. Defining Hilbert space $\mathbf{L}^2(\Omega_s)$ corresponding to $[L^2(\Omega_s)]^2$ for 2D-DIC and $[L^2(\Omega_s)]^3$ for SDIC, this yields,

$$\mathbf{u}_k^\star = \underset{\mathbf{u}_k \in \mathbf{L}^2(\Omega_s)}{\arg\min} \sum_{c=1}^{n_c} \int_{\Omega_s} \left(r_k^c(\mathbf{u}_k, \mathbf{x}) \right)^2 d\mathbf{x} \tag{4}$$

These least square problems are non-linear. Assuming that $\mathcal{I}_k^c$ (and thus $\mathcal{I}_0^c$) are differentiable $\forall c$ and $\forall k$, a Gauss-Newton algorithm can be implemented for the resolution [14]. At each time t_k, we consider that we have a good approximation of $\mathbf{u}_k^\star$ denoted by $\mathbf{u}_k$. Only a correction $\delta\mathbf{u}_k$ over this initialization is sought. The linearization reads:

$$r_k^c(\mathbf{u}_k + \delta\mathbf{u}_k, \mathbf{x}) \approx r_k^c(\mathbf{u}_k, \mathbf{x}) + \delta\mathbf{u}_k^\top \, \mathbf{J}^{c\top} \, \boldsymbol{\nabla}\mathcal{I}^c \tag{5}$$

where $\mathbf{J}^c = \mathrm{Jac}_{\mathbf{x}}(\mathbf{p}^c)(\mathbf{x}+\mathbf{u}_k)$ is the Jacobian of the camera projector (which admits an analytical expression when using a parametric distortion model) and $\boldsymbol{\nabla}\mathcal{I}^c = \mathrm{Grad}_{\mathbf{y}}(\mathcal{I}_k^c)(\mathbf{p}^c(\mathbf{x}+\mathbf{u}_k))$ is the image gradient interpolated at pixel position $\mathbf{p}^c(\mathbf{x}+\mathbf{u}_k)$. The approximation $\boldsymbol{\nabla}\mathcal{I}^c \approx \mathrm{Grad}_{\mathbf{y}}(\mathcal{I}_0^c)(\mathbf{p}^c(\mathbf{x}))$, which is often used to avoid multiple assembly of the left hand side operator in the context of small rotations [23], is adopted in this work. Finally, the unknown displacement correction $\delta\mathbf{u}_k$ (and so the displacement $\mathbf{u}_k$) is sought in an approximation subspace:

$$\delta\mathbf{u}_k = \sum_{i=1}^{n_s} q_i^k \boldsymbol{\psi}_i(\mathbf{x}) \tag{6}$$

$\boldsymbol{\psi}_i(\mathbf{x})$ is a set of n_s well chosen basis functions and q_i^k denote the corresponding degrees of freedom (dof) at time step k. In this paper, finite element shape functions are used in order to benefit from a common formalism with numerical simulation [35]. By introducing this approximation into the linearized minimization problem and performing the differentiation, we finally obtain the following linear system to be solved at each iteration of the Gauss-Newton algorithm and for each time step k:

$$\mathbf{M}\,\mathbf{q}^k = \mathbf{b}^k(\mathbf{u}_k) \tag{7}$$

where $\mathbf{q}^k$ is the dof vector and $\forall (i,j) \in \{1,..,n_s\}^2$:

$$[\mathbf{M}]_{ij} = \sum_{c=1}^{n_c} \int_{\Omega_s} \boldsymbol{\psi}_i(\mathbf{x})^\top \mathbf{J}^{c\top} \boldsymbol{\nabla}\mathcal{I}^c \boldsymbol{\nabla}\mathcal{I}^{c\top} \mathbf{J}^c \boldsymbol{\psi}_j(\mathbf{x}) \, d\mathbf{x} \tag{8}$$

$$\left[\mathbf{b}^k(\mathbf{u})\right]_i = -\sum_{c=1}^{n_c} \int_{\Omega_s} \boldsymbol{\psi}_i(\mathbf{x})^\top \mathbf{J}^{c\top} \boldsymbol{\nabla}\mathcal{I}^c \; r_k^c(\mathbf{u}, \mathbf{x}) \, d\mathbf{x} \tag{9}$$

Because of the short variations of the image gradient, the quadrature of the above integral is performed using a Riemann sum with respect to the pixel partition. A dedicated quadrature rule was proposed in [29] and further enhanced in [28] for multiple camera and/or non-linear camera models.

3 The proposed space-time PGD-DIC formulation

As an alternative, the purpose of this work is to build a resolution scheme based on the use of some variable separation techniques widely encountered in numerical simulations [2,25,19,12,10,42]. The interest of extending such methods to DIC has already been illustrated in previous works [27,17], where the dimensions of space were separated in order to speedup computation time. In this work, the idea is to separate space and time in the evolution problem of DIC (1). It will be shown that prescribing smooth or physically sound time evolution, acts as a regularization of the inverse problem of space-time full-field measurements. This strategy is presented below.

The starting point uses a global formulation written as a least-square problem over the space-time domain, as proposed by [6,8,24]. In order to do this, we introduce the functional spaces $\mathcal{T} = L^2(\Omega_t)$ and $\mathbf{L}^2\big(\Omega_t;\mathbf{L}^2(\Omega_s)\big) = \mathbf{L}^2(\Omega_s)\otimes\mathcal{T}$ and we look for the space-time solution as follows:

$$\mathbf{u}^\star(\mathbf{x},t) = \underset{\mathbf{u}\in\mathbf{L}^2(\Omega_t;\mathbf{L}^2(\Omega_s))}{\arg\min} \sum_{c=1}^{n_c} \int_{\Omega_t}\int_{\Omega_s} \Big(r^c(\mathbf{u}(\mathbf{x},t),\mathbf{x},t)\Big)^2 \, d\mathbf{x}\; dt \tag{10}$$

It should be noted that, because of the time discretization of images $\mathcal{I}^c(t)$, a rectangle method is used in practice for the quadrature over the time domain. For an arbitrary time dependent quantity, a, we perform the following computation to integrate over time:

$$\int_{\Omega_t} a(t)\; dt = \frac{1}{f}\sum_{k=1}^{n_t} a(t_k)$$

where f is the acquisition frame rate.

3.1 Separated representation and time regularization

From formulation (10), the crucial point of the proposed strategy is to consider a rank-m space-time separated approximation for the solution of the evolution problem [19,27]:

$$\mathbf{u}(\mathbf{x},t) = \sum_{n=1}^{m} \mathbf{v}_n(\mathbf{x})\cdot\lambda_n(t) \tag{11}$$

Here, both $\mathbf{v}_n$ and λ_n are unknown *a priori*. Regarding the approximation of space functions $\mathbf{v}_n$, a classical finite element discretization is adopted, the same as for displacement $\mathbf{u}_k$ in the incremental approach (see Eq. (6)):

$$\mathbf{v}_n(\mathbf{x}) = \sum_{i=1}^{n_s} q_i^n \boldsymbol{\psi}_i(\mathbf{x}) \tag{12}$$

The interest of form (11) is that a mechanically sound expression can be adopted for the temporal evolution $\lambda_n(t)$ of the space-time solution. The number of images acquired during quasi static tests being large, the evolution of mechanical fields can be fairly smooth relative to framerate. Thus smooth approximation

subspaces of dimension $n_\tau << n_t$ can be chosen to describe the time evolution of the displacement:

$$\lambda_n(t) = \sum_{j=1}^{n_\tau} p_j^n \phi_j(t), \tag{13}$$

where $\phi_j^n(t)$ can denote either Finite Elements [6] or smoother approximations such as B-splines in time, and p_j^n represents the corresponding parameters or degrees of freedom. Thus, by reducing the number of unknowns in time with a constant number of image data, the noise sensitivity should be reduced.

Without loss of generality, we will simply consider a rank one approximation in the remainder of the paper, since, following [27,17], a rank m approximation is obtained in a greedy manner from successive best rank-one approximations. In addition, in the particular case of linear vibrations, a rank one approximation may be sufficient. Hence, the space-time displacement is sought as:

$$\mathbf{u}(\mathbf{x}, t) = \mathbf{v}(\mathbf{x}) \cdot \lambda(t) \tag{14}$$

In the context of linear vibrations, we know that the time function λ is harmonic. A more physically sound approximation can be used in this particular situation. This approximation involves only two unknowns: the phase, ϕ, and the pulsation, ω, of the harmonic signal. They can be brought together in one vector $\mathbf{p} = [\ \omega \quad \phi\ ]^\top$. In this paper, which investigates the case of linear vibrations as a first illustration, it is proposed to look for a temporal representation in the following form:

$$\lambda(t, \mathbf{p}) = \sin(\omega\ t + \phi) \tag{15}$$

3.2 Fixed point resolution

By substituting form (14) into problem (10), the separated time-space DIC problem can be recast as:

$$\left(\mathbf{v}^\star, \lambda^\star\right) = \underset{(\mathbf{v},\lambda)\in\mathbf{L}^2(\Omega_s)\otimes\mathcal{T}}{\arg\min} \sum_{c=1}^{n_c} \int_{\Omega_t} \int_{\Omega_s} \left(r^c(\mathbf{v}(\mathbf{x}) \cdot \lambda(t), \mathbf{x}, t)\right)^2 d\mathbf{x}\ dt \tag{16}$$

Because of the product of unknowns, the problem is solved with an alternating direction fixed point strategy. Note that the algorithm proposed in the following is based on developments regarding existing PGD methods in structural [25][19] and experimental mechanics [27][17]. In order to do this, two mappings are defined:

1. $\mathbf{S} : \mathcal{T} \to \mathbf{L}^2(\Omega_s)$ is the application that maps a time function λ into a space function $\mathbf{v} = \mathbf{S}(\lambda)$. It is associated with the minimization of (16) with respect to $\mathbf{v}(\mathbf{x})$ with $\lambda(t)$ being fixed. This problem is referred to as the *space problem*.
2. $\mathbf{T} : \mathbf{L}^2(\Omega_s) \to \mathcal{T}$ is the application that maps a space function $\mathbf{v}$ into a time function $\lambda = \mathbf{T}(\mathbf{v})$. It is associated with the minimization of (16) with respect to $\lambda(t)$ with $\mathbf{v}(\mathbf{x})$ being fixed. This problem is referred to as the *time problem*.

A $(\mathbf{v}, \lambda)$ pair verifies (16) if and only if $\mathbf{v} = \mathbf{S}(\lambda)$ and $\lambda = \mathbf{T}(\mathbf{v})$. For the n^{th} iteration of the fixed point algorithm, we thus proceed as follows: starting from an initial time function $\lambda^{(0)} \in \mathcal{T}$, we look for $\mathbf{v}^{(n)} \in \mathbf{L}^2(\Omega_s)$ and $\lambda^{(n)} \in \mathcal{T}$ such that: $\mathbf{v}^{(n)} = \mathbf{S}(\lambda^{(n-1)})$ and $\lambda^{(n)} = \mathbf{T}(\mathbf{v}^{(n)})$. The resolutions associated with the two mappings, $\mathbf{S}$ and $\mathbf{T}$, are detailed below.

3.2.1 Space correlation problem

First, the space problem corresponding to application $\mathbf{S}$ is formulated. It reads:

$$\mathbf{v}^\star = \underset{\mathbf{v}\in\mathbf{L}^2(\Omega_s)}{\arg\min} \sum_{c=1}^{n_c} \int_{\Omega_t}\int_{\Omega_s} \left(r^c(\mathbf{v}(\mathbf{x})\cdot\lambda(t),\mathbf{x},t)\right)^2 d\mathbf{x}\; dt, \quad \lambda(t) \text{ considered fixed.} \tag{17}$$

As for classic DIC, a Gauss-Newton algorithm is used for the minimization (17). Since all the functions of time are known, the time integral of (17) can be computed, and we are left with a modified static DIC problem. The linearization and differentiation are similar to usual FE-DIC and SDIC. Starting from an initial guess $\mathbf{v}^0$, the following linear system is obtained for the Gauss-Newton update:

$$\mathbf{M}_s\; \delta\mathbf{q} = \mathbf{b}_s(\mathbf{v}^0,\mathbf{p}), \tag{18}$$

where the operators read:

$$\mathbf{M}_s = \frac{1}{f}\mathbf{M}\; \sum_{k=1}^{n_t} \lambda^2(t_k) \tag{19}$$

$$\mathbf{b}_s(\mathbf{v}^0,\lambda) = \frac{1}{f}\sum_{k=1}^{n_t} \lambda(t_k)\; \mathbf{b}^k(\mathbf{v}^0(\mathbf{x})\lambda(t_k,\mathbf{p})) \tag{20}$$

and where $\delta\mathbf{q}$ is a vector that groups together the degrees of freedom associated with correction $\delta\mathbf{v}$. Note that the operator $\mathbf{M}_s$ and right hand side $\mathbf{b}_s$ can be easily computed from the operator $\mathbf{M}$ and right hand sides $\mathbf{b}^k$ of the incremental approach, see Eqs. (8) and (9).

3.2.2 Time correlation problem

For application $\mathbf{T}$, the unknown $\mathbf{p}$ is sought to estimate the temporal function $\lambda(t,\mathbf{p})$ (see Eq. (15)). The associated problem reads:

$$\mathbf{p}^\star = \underset{\mathbf{p}\in\mathbf{R}^2}{\arg\min} \sum_{c=1}^{n_c} \int_{\Omega_t}\int_{\Omega_s} \left(r^c(\mathbf{v}(\mathbf{x})\cdot\lambda(t,\mathbf{p}),\mathbf{x},t)\right)^2 d\mathbf{x}\; dt, \quad \mathbf{v}(\mathbf{x}) \text{ considered fixed.} \tag{21}$$

Once again, a Gauss-Newton algorithm is performed for the resolution. Starting from an initial guess $\mathbf{p}^0$, we search for a correction $\delta\mathbf{p}$ over this approximation. The linearization and differentiation lead to the following linear system:

$$\mathbf{M}_t\; \delta\mathbf{p} = \mathbf{b}_t(\mathbf{v},\mathbf{p}^0), \tag{22}$$

where:

$$\mathbf{M}_t = \mathbf{q}^\top\mathbf{M}\;\mathbf{q}\; \sum_{k=1}^{n_t} \boldsymbol{\nabla}\lambda\boldsymbol{\nabla}\lambda^\top \tag{23}$$

$$\mathbf{b}_t(\mathbf{v},\mathbf{p}^0) = \sum_{k=1}^{n_t} \boldsymbol{\nabla}\lambda\; \mathbf{q}^\top\mathbf{b}^k(\mathbf{v}(\mathbf{x})\lambda(t_k,\mathbf{p}^0)) \tag{24}$$

and where the gradient of the time function reads:

$$\boldsymbol{\nabla}\lambda = \begin{bmatrix} t\ \cos(\omega\ t + \phi) \\ \cos(\omega\ t + \phi) \end{bmatrix}$$

Remark. If finite elements had been used for the discretization in time, this gradient would have simply consisted of the time shape functions $\phi_j(t)$. Therefore, $\mathbf{M}_t$ would have represented a temporal mass matrix (of unit density) multiplied by the scalar $\mathbf{q}^\top \mathbf{M}\ \mathbf{q}$. Once again, we emphasize that the new operators $\mathbf{M}_t$ and $\mathbf{b}_t$ are easily obtained from the incremental operators $\mathbf{M}$ and $\mathbf{b}$. Therefore another attractive feature of the proposed method is that the extra implementation effort, starting from a classic global DIC code, is only slight. The method is non-intrusive with respect to image manipulations and finite element routines. As mentionned in the introduction, the proposed PGD-DIC method could well be applied to a sub-set approach.

3.3 Initialization

As any Newton-like algorithm, a relevant initial approximation is required to ensure convergence. Frequency $\omega/(2\pi)$ is generally precisely known because of the instrument providing the harmonic excitation (an accelerometer or a single point laser vibrometer). In addition, the initial phase, ϕ, and mode shape, $\mathbf{q}$, are estimated, in this work, from a first Fourier analysis of the image series using the incremental approach.

3.4 Reference image

The set of reference images $\mathcal{I}_0^c$ is usually taken before shaking the structure. This is required, at least in SDIC in order to perform the initial shape measurement. Unfortunately, the initial configuration may not exactly correspond to the centre of the harmonic mode (where $\lambda = 0$). There might be some rigid body translations and rotations that must be accounted for. This is the case, for instance, when the specimen is set on a shaking table. In this situation, an additional unknown $\boldsymbol{\alpha}$ representing the amplitude of the initial rigid body (six associated dofs) is introduced. The solution is sought as a rank-2 PGD approximation:

$$\mathbf{u}(\mathbf{x}, t) = \mathbf{v}(\mathbf{x}) \cdot \lambda(t) + \mathbf{R}(\mathbf{x})\ \boldsymbol{\alpha} \tag{25}$$

where $\mathbf{R}(\mathbf{x})$ constitutes a basis of rigid body modes.

Moreover, reference images can also be taken during the shaking. In this case, the time evolution of the nodal displacement is the sum of a harmonic evolution and a shift p, which constitutes an additional unknown.

$$\lambda(t, \mathbf{p}) = \sin(\omega\ t + \phi) + p \tag{26}$$

Finally, a block-diagram summarizing the different stages of the proposed strategy is presented in Figure 1.

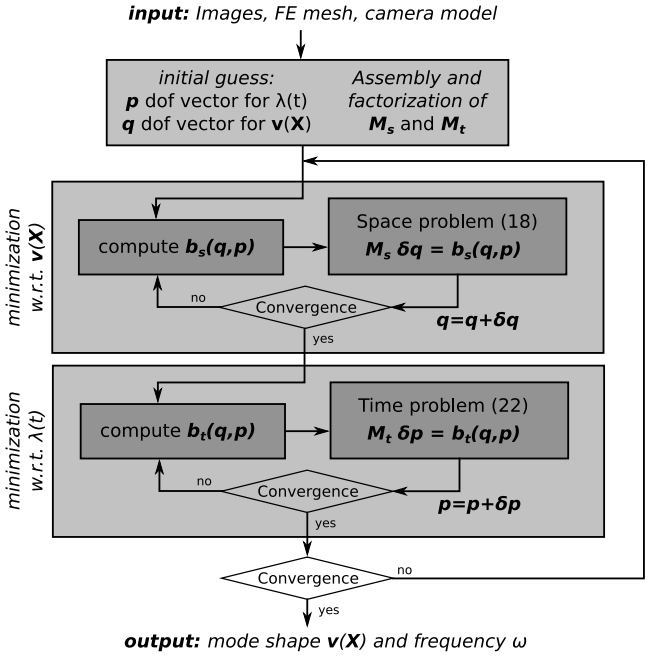

Fig. 1 Scheme of the proposed method. After initialization, assembly and factorisation of the operators, the method consists of an alternating fixed point minimization with respect to space (first block) and time (second block). The minimisation with respect to space (respectively time) is done iteratively (Gauss Newton), assuming time (resp. space) function is fixed.

4 Examples

4.1 2D DIC example

4.1.1 Experimental setup

As a first illustration of the proposed method, the eigenmodes of a clamped-free beam are analysed using 2D-DIC. The experimental set-up is shown in Figure (2). More precisely, the specimen was an aluminium beam of length 273 mm and of rectangular section 20× 40 mm. The material parameters (Young's modulus $E = 69$ GPa, Poisson's ratio $\nu = 0.29$ and density $\rho = 2698$ kg.m^{-3}) were taken from the literature. The beam was clamped on a shaking table. A sine sweep was performed initially to locate the eigenfrequencies approximately. Then a second sweep was performed and the shaker was held in the first two previously identified bending modes. One accelerometer was placed on the top of the beam and one on the table to monitor the experiment. Since we are only interested in the in-plane bending modes in this section, one single front parallel Photron Fastcam SA3 high speed camera was used to take the images. The camera was positioned outside the passively isolated foundations and also outside the soundproofing enclosure in which the vibrating table is installed. This avoids vibro-acoustic disturbances in the camera. The frame rate was 2000 Hz with an image definition of 1024×128 px. A black and white speckle was sprayed on the specimen in order to provide a

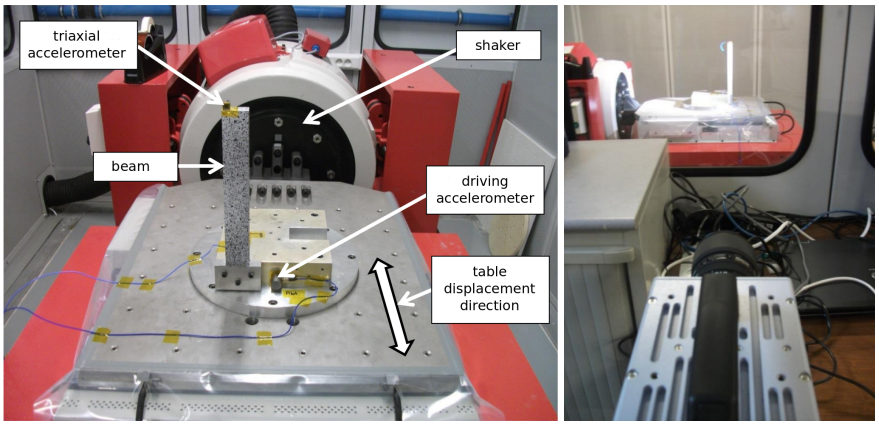

Fig. 2 Experimental setup (left) for the 2D case with one front parallel camera (right).

random texture suitable for the DIC. Two sides were speckled to analyse bending modes in both directions. Only one direction is analysed herein. One Dedolight (400 W) spot was found to provide sufficient illumination.

Note that a fixed harmonic excitation was considered during the tests. The analysed data set does not make it possible to estimate the damping. Damping ratio evaluation is another problem to which such algorithms could be applied, but this was not done in this study.

4.1.2 Incremental DIC analysis

To start with, a series of 86 images was analysed using the incermental approach (see Section 2). Figure 3 (top) presents the maps of the measured displacements, $\mathbf{u}_k$, of 9 equally spaced time steps, corresponding to 9 consecutive images. This set of time steps corresponds to approximately to one period of vibration of the first vibration mode. It can be observed that, when the beam moves on the left, the displacement is noisy (displacement is amplified by a factor 30) for 2 of the 9 images. Note that this issue could have been avoided by using larger elements or any other regularization technique [30,27,31,11] but it was allowed to persist as it enabled the effect of noise on mode measurement, to be visualized. The 7 other displacements were far less noisy. In addition, it can be clearly seen that this noise in not harmonic at all. This is obvious and explains why prescribing harmonicity should act as a physical regularization.

4.1.3 A posteriori *mode measurement*

In order to measure the mode shape, a first naive approach was to perform a Least Square (LS) projection of these previously measured fields $\{\mathbf{u}_k\}$ on a space-time separated representation $\mathbf{v}(\mathbf{x}) \cdot \lambda(t)$. Actually, it was not a regularization of the measurement, but rather an *a posteriori* filtering method. More precisely, it consisted of solving the following problem, see [26]:

$$(\mathbf{v}^\star, \lambda^\star) = \underset{(\mathbf{v},\lambda)\in \mathbf{L}^2(\Omega_s)\otimes\mathcal{T}}{\arg\min} \sqrt{\sum_k \|\mathbf{u}_k(\mathbf{x}) - \mathbf{v}(\mathbf{x})\cdot\lambda(t_k)\|_2^2} \tag{27}$$

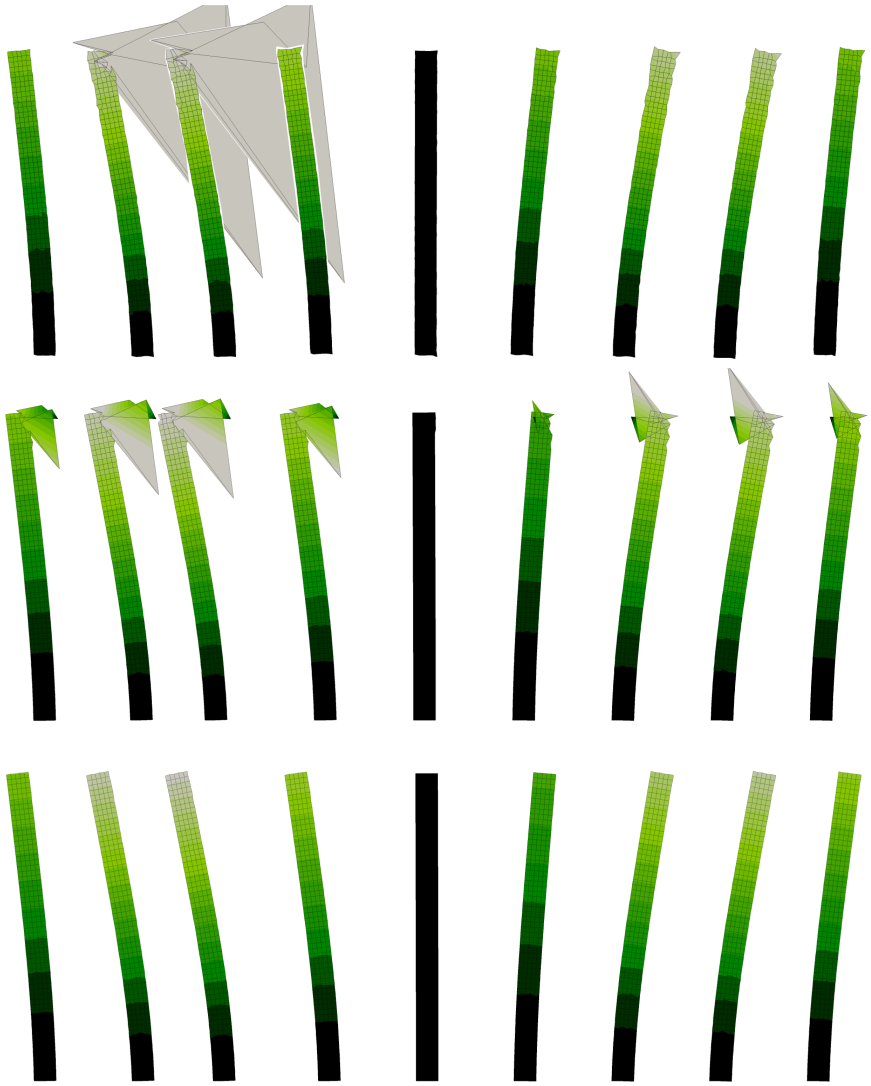

Fig. 3 (top) Incrementally measured displacements over one period ; (middle) *LS*-projection of the incrementally measured displacements and reconstruction of displacements over one period; (bottom) Proposed separated time-space modal measurement reconstructed over one period. (amplification factor: 30)

This nonlinear Least-Square (LS) problem was solved using another fixed point algorithm. The minimization with respect to the space function was straightforward; the minimization with respect to time function was still nonlinear and was solved using a dedicated Gauss-Newton algorithm.

The resolution of this problem yielded a mode shape $\mathbf{v}^{LS}$ along with the parameters of the sine function λ^{LS}. Figure 3 (middle) shows the reconstruction of the product $\mathbf{v}^{LS} \cdot \lambda^{LS}$ over the same period. It can be clearly seen that the noise is decreased when this least-square filtering technique is used. However, it can also

be noticed that the noise is spread over the full period, which is due to the fact that the noise is made harmonic. As such, the noise is actually reduced for the two problematic time steps, but it is largely increased for the other seven time steps.

4.1.4 A priori *mode measurement using PGD-DIC*

As a remedy for the aforementioned issue, the proposed time-space separated DIC approach is now applied to the same dataset using the same FE mesh. Consequently, only the formulation on the space-time domain differs (see Section 3). From the images, this method directly yields a pair of space $\mathbf{v}^{Sep}$ and time λ^{Sep} functions. The PGD algorithm is initialized with the noisy mode estimated with the previous least-square approach.

Figure 3(bottom) presents the reconstruction of the space-time solution $\mathbf{v}^{Sep} \cdot \lambda^{Sep}$ over one period. The displacement is definitely less noisy over the whole time interval. These results demonstrate that time-space tensor approximation acts as a physical regularization technique in the space-time DIC minimization problem.

A plane stress finite element model of the specimen was built. The measured and simulated eigen frequencies are compared to the closed form of an Euler Bernoulli clamped-free beam in Table 1. Firstly, it can be seen that the mesh

ine accelerometer	proposed FE-DIC	FE model	beam theory
ine 195.23 Hz	194.72 Hz	221.15 Hz	219.2 Hz
ine			

Table 1 Comparison of measured and simulated eigenfrequencies

is sufficiently fine to be close to the beam theory. Secondly, it appears that the frequency measured using the proposed method is in good agreement with the accelerometer. It also seems that the FE and analytical frequencies overestimate the actual vibration mode, certainly because of the use of approximate elastic parameters. This mismatch could be used to update the mechanical parameters using a space-time integrated approach [20, 24, 22]. Finally, the simulated and measured mode shapes were compared using a Modal Insurance Criterion (MAC) matrix. Using a DIC method based on Finite Elements, the MAC matrix computation is straightforward and the same mesh was used here for both the simulation and the measurement. The MAC matrix could then be computed directly by taking the scalar product between the experimental and simulated dof vectors. For instance, the MAC matrix corresponding to the first two bending modes of the beam is depicted in Figure 4. It exhibits a relatively good correlation between computed and measured mode shapes.

4.2 SDIC example

4.2.1 Experimental setup

In this section, we apply the methodology to the more complex case of the SDIC measurement of the out-of-plane bending mode of an accelerated fatigue specimen.

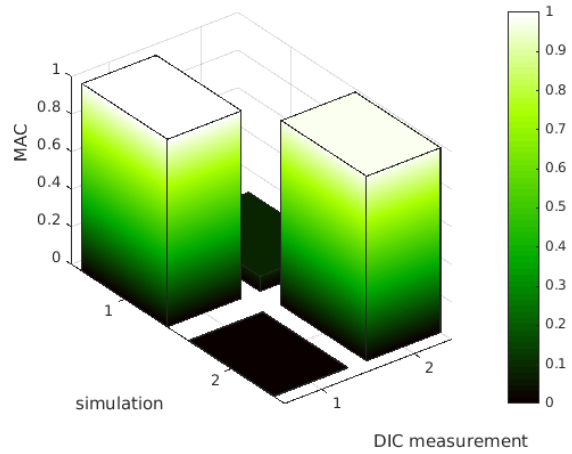

Fig. 4 MAC matrix for the first two bending modes of the beam

The 170 ×90 × 2 mm stainless steel specimen ($E = 197$ GPA, $\nu = 0.3$, $\rho = 7990$ kg.m^{-3}) is clamped at the bottom (see Fig. 5(left)). The shape of the specimen was designed to have a bending mode around 1 kHz which would exhibit pure bending in a region of interest located at the top. The specimen was mounted on

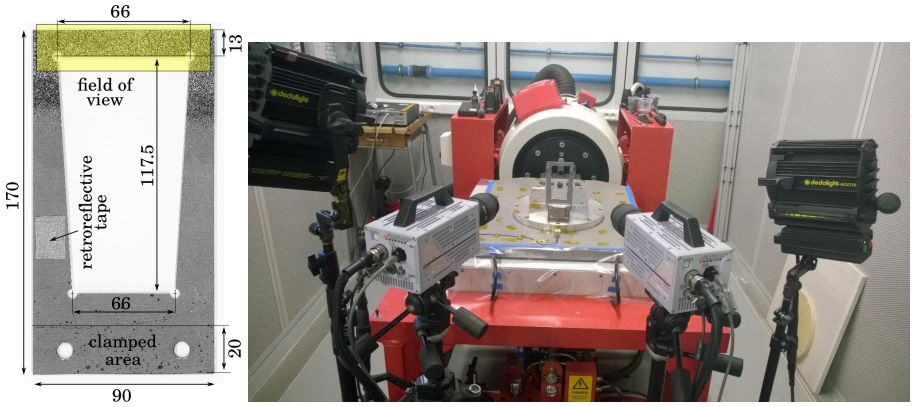

Fig. 5 Experimental setup: dimensions of the fatigue specimen (left) for the stereo case; instrumentation with two high speed cameras, two Dedolights and one single point laser vibrometer (right).

the same shaking table as previously. A pair of reference images were taken before the experiment using two high speed digital cameras, see Figure 6. They were taken as reference images for the space-time SDIC problem and were also used to estimate the gap between the theoretical and actual shape, in order to correct the shape of the SDIC mesh, following [4,28]. As shown in Figure 7, the observed surface was almost flat. The estimated waviness did not exceed 30 microns, which is consistent with the manufacturing specification for the specimen.

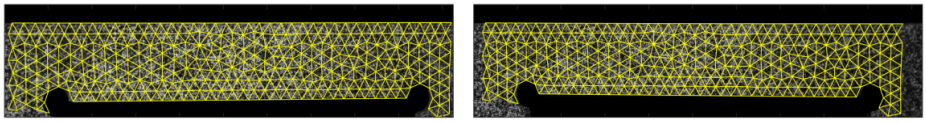

Fig. 6 Projection of the finite element mesh vertices in the left and right reference images.

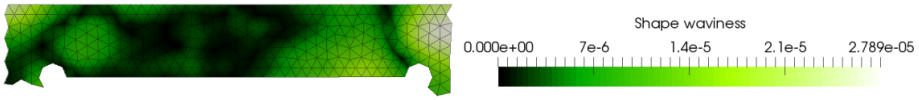

Fig. 7 Shape measurement: magnitude of the discrepancy between model and specimen (m).

After a first frequency sweep used to locate the mode of interest, the shaker was held at the frequency of 1033 Hz. To do this, the test was monitored with a single point laser accelerometer, see the retroreflective tape on Figure 5(left). Two series of stereo images were taken by a pair of high-speed cameras. This double image set was used to perform a stereo measurement of the vibration modes at a framerate of 2000 Hz and at image definition of 1024×128 px.

In addition, a finite element model was built in ABAQUS[1] using shell 3 node triangular elements. The modal analysis predicted an eigenmode at 1062 Hz. The corresponding mode shape is depicted in Figure 8.

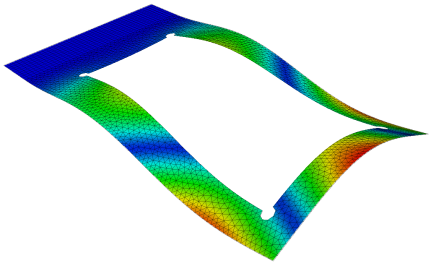

Fig. 8 Eigenmode at 1062 Hz computed using an ABAQUS shell model

4.2.2 Analysis using time-space PGD-DIC

The proposed space-time PGD-DIC method was then applied to the image sets. The eigenfrequency estimated by the image analysis was 1033.71 Hz, which is comparable to the laser measurement of 1033.7 Hz. The measured mode shape was also in good agreement with the simulated mode, see Figure 9. The benefit of the proposed space-time PGD approach over a more classic incremental DIC can be seen by simply looking at the measured mode shapes. Figure 10 (left) presents the displacement measurement using incremental DIC. The number of unknowns equals the number of space unknowns multiplied by the number of

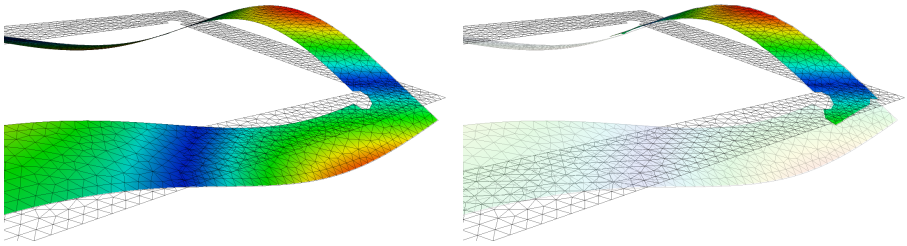

Fig. 9 Comparison between the simulated (left) and identified (right) eigenmodes

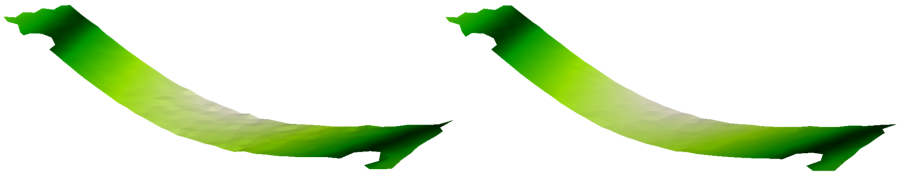

Fig. 10 Comparison between the mode measured using the incremental formulation (left) and the one measured using space-time PGD-DIC (right), which seems more regular.

time steps $n_s \times n_t$. Conversely, with the proposed PGD approach, the number of unknowns is drastically decreased to $n_s + n_\tau$ (n_τ being the dimension of the time approximation subspace), which enables the measurement to be regularized and its uncertainty to be reduced, see Figure 10(right).

4.2.3 Toward the use of low speed equipment

Lastly, it is worth noting that such a space-time separated framework may help to reduce the measurement uncertainties even further since it lightens the trade-off between framerate and image definition. Similarly to [38,40], we show, in this section, that by assuming a regular evolution in time, it becomes possible to significantly reduce the acquisition framerate. This may offer the opportunity to use non-specific devices like low speed asynchronous imaging [38,40]. The benefit of this is that it substantially improves the definition of the images. The measurement resolution (being closely related to image definition) is also improved.

As a first proof of concept, the method is applied to the same set of images, but, this time, only 1 in every 20 images is considered, which simulates an acquisition framerate of 100 Hz, see Figure 11. This time the eigenfrequency measured by

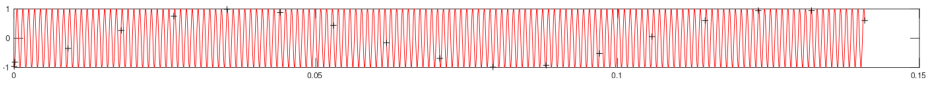

Fig. 11 Comparison of the evolution of the displacement of one point in the zone of interest using the incremental approach (black +) and the space-time formulation (red)

the laser is considered fixed, otherwise the solution would not be unique. This assumption that the eigenfrequency is reliable is not a very restrictive one, since at least one single point laser or accelerometer is required to monitor the experiment while it is in progress. Again, with only 17 analysed images, the displacement map is much less noisy when the space-time PGD is used as a space regularization technique, as compared to the incremental approach, see Figure 12. Obviously

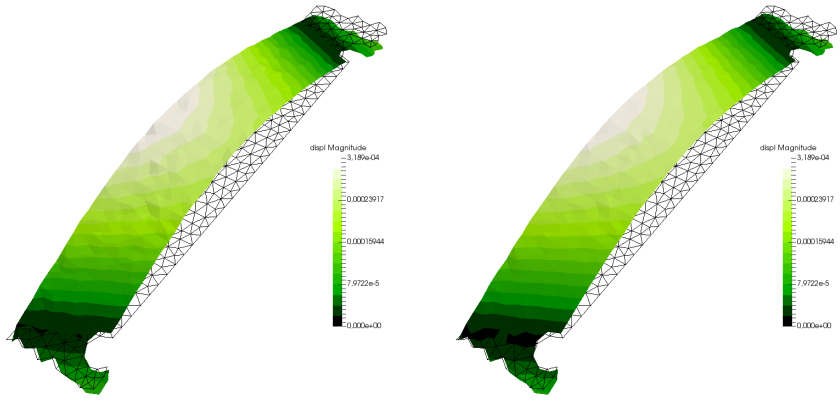

Fig. 12 Comparison between the measured mode using the incremental formulation (left) and the one obtained using asynchronous PGD-DIC (right) which again apprears more regular.

such a method should reduce the measurement uncertainties even further because, thanks to the reduction of the frame rate by a factor of 20, it will be possible to acquire images of significantly higher definition.

5 Conclusion

A new method has been proposed for the measurement of displacement fields during dynamic tests using FE-DIC, both in 2D and in Stereo. In such a situation, high speed cameras are classically used to provide an image series, where each image pair is analysed independently. It was shown in the examples that the noise obtained during such incremental DIC measurements is propagated in the sinusoidal fitting used to estimate the mode shape, *a posteriori* [38]. This Finite Element Model Updating (FEMU)-like two-step approach to identifying the vibration mode actually spreads and propagates noise instead of reducing it. To avoid these issues, an *integrated*-like method is developed in this work. It starts from a general writing of the space-time problems of DIC, DVC and SDIC which also constitutes a novelty of this paper. Then, the key point is to search the space-time displacement as a product of separate functions of space and time. Using this formulation, we finally prescribe time regularity in the resolution of the DIC problem over the full space-time domain, which also behaves as a mechanical regularization in the space domain. Such a method has many advantages, *including*:

1. It offers the possibility to use time regularity to improve space field uncertainties.
2. It can alleviate the trade-off between framerate and image definition, since low speed equipment can be used.
3. The additional implementation effort with respect to an existing global DIC code is very small. The method only involves products and scalar products of classic DIC operators with dof vectors or operators. There is no need to modify the functions at the finite element level.
4. As was done in this simple case of linear vibrations for the rigid body modes, it is possible to consider higher rank approximations for non-periodic evolutions. For instance, more generic time basis functions could be used, such as typical Lagrange polynomials or more recent B-spline functions. In this case, the algorithm would be quite similar to the PGD-DIC method developed in [27]. To estimate the separability of the space-time field (and therefore the efficiency of the PGD approach), it is possible to compute the Singular Value Decomposition (SVD) of a field derived from a classic DIC software.

References

1. ABAQUS/Standard User's Manual, Version 6.9 Providence, RI : Simulia, (2009)
2. Ammar, A., Mokdad, B., Chinesta, F., Keunings, R.: A new family of solvers for some classes of multidimensional partial differential equations encountered in kinetic theory modeling of complex fluids. Journal of Non-Newtonian Fluid Mechanics **139**(3), 153–176 (2006)
3. Balcaen, R., Reu, P., Lava, P., Debruyne, D.: Stereo-dic uncertainty quantification based on simulated images. Experimental Mechanics **57**(6), 939–951 (2017)
4. Beaubier, B., Dufour, J., Hild, F., Roux, S., Lavernhe, S., Lavernhe-Taillard, K.: Cad-based calibration and shape measurement with stereodic - principle and application on test and industrial parts. Experimental Mechanics **54**(3), 329–341 (2014)
5. Beberniss, T., Eason, T., Spottswood, S.: High-speed 3d digital image correlation measurement of long-duration random vibration; recent advancements and noted limitations. In: International Conference on Noise and Vibration Engineering (ISMA), Katholieke Universiteit Leuven, Belgium (2012)
6. Besnard, G., Guerard, S., Roux, S., Hild, F.: A space-time approach in digital image correlation: Movie-dic. Opt. Lasers Eng. **49**, 71–81 (2011)
7. Besnard, G., Hild, F., Roux, S.: finite-element displacement fields analysis from digital images: Application to Portevin-le Châtelier bands. Experimental Mechanics **46**(6), 789–803 (2006)
8. Besnard, G., Leclerc, H., Roux, S., Hild, F.: Analysis of image series through digital image correlation. Journal of Strain Analysis for Engineering Design **47**(4), 214–228 (2012)
9. Bornert, M., Brémand, F., Doumalin, P., Dupré, J.C., Fazzini, M., Grédiac, M., Hild, F., Mistou, S., Molimard, J., Orteu, J.J., Robert, L., Surrel, Y., Vacher, P., Wattrisse, B.: Assessment of digital image correlation measurement errors: methodology and results. Experimental Mechanics **49**(3), 353–370 (2009)
10. Bouclier, R., Louf, F., Chamoin, L.: Real-time validation of mechanical models coupling pgd and constitutive relation error. Computational Mechanics **52**(4), 861–883 (2013)
11. Bouclier, R., Passieux, J.C.: A domain coupling method for finite element digital image correlation with mechanical regularization: Application to multiscale measurements and parallel computing. International Journal for Numerical Methods in Engineering **111**(2), 123–143 (2017)
12. Chinesta, F., Leygue, A., Bordeu, F., Aguado, J., Cueto, E., Gonzalez, D., Alfaro, I., Ammar, A., Huerta, A.: Pgd-based computational vademecum for efficient design, optimization and control. Archives of Computational Methods in Engineering **20**(1), 31–59 (2013)
13. Dufour, J.E., Beaubier, B., Hild, F., Roux, S.: Cad-based displacement measurements with stereo-dic. Experimental Mechanics **55**(9), 1657–1668 (2015)

14. Fehrenbach, J., Masmoudi, M.: A fast algorithm for image registration. Comptes Rendus Mathématique **346**(9-10), 593–598 (2008)
15. Fruehmann, R.K., Dulieu-Barton, J.M., Quinn, S., Tyler, J.P.: The use of a lock-in amplifier to apply digital image correlation to cyclically loaded components. Optics and Lasers Engineering **68**, 149–159 (2015)
16. Garcia, D., Orteu, J.J., Penazzi, L.: A combined temporal tracking and stereo-correlation technique for accurate measurement of 3d displacements: Application to sheet metal forming. Journal of Materials Processing Technology **125-126**, 736–742 (2002)
17. Gomes Perini, L., Passieux, J.C., Périé, J.N.: A multigrid PGD-based algorithm for volumetric displacement fields measurements. Strain **50**(4), 355–367 (2014)
18. Helfrick, M.N., Niezrecki, C., Avitabile, P., Schmidt, T.: 3D digital image correlation methods for full-field vibration measurement. Mechanical Systems and Signal Processing **25**(3), 917–927 (2011)
19. Ladevèze, P., Passieux, J.C., Néron, D.: The LATIN multiscale computational method and the Proper Generalized Decomposition. Computer Methods in Applied Mechanics and Engineering **199**(21), 1287–1296 (2010)
20. Leclerc, H., Périé, J.N., Roux, S., Hild, F.: Integrated digital image correlation for the identification of mechanical properties. Lectures Notes in Computer Sciences **5496**, 161–171 (2009)
21. Lucas, B., Kanade, T.: An iterative image registration technique with an application to stereo vision. In: Proceedings of Imaging Understanding Workshop, pp. 121–130 (1981)
22. Mathieu, F., Leclerc, H., Hild, H., Roux, S.: Estimation of elastoplastic parameters via weighted FEMU and intergrated DIC. Experimental Mechanics **55**(1), 105–119 (2015)
23. Neggers, J., Blaysat, B., Hoefnagels, J.P.M., Geers, M.G.D.: On image gradients in digital image correlation. International Journal for Numerical Methods in Engineering **105**, 243–260 (2016)
24. Neggers, J., Hoefnagels, J.P.M., Geers, M.G.D., Hild, F., Roux, S.: Time-resolved integrated digital image correlation. International Journal for Numerical Methods in Engineering **103**(3), 157–182 (2015)
25. Nouy, A.: A generalized spectral decomposition technique to solve a class of linear stochastic partial differential equations. Computer Methods in Applied Mechanics and Engineering **196**(45-48), 4521–4537 (2007)
26. Passieux, J.C., Ladevèze, P., Néron, D.: A scalable time-space multiscale domain decomposition method: adaptive time scale separation. Computational Mechanics **46**(4), 621–633 (2010)
27. Passieux, J.C., Périé, J.N.: High resolution digital image correlation using Proper Generalized Decomposition: PGD-DIC. International Journal for Numerical Methods in Engineering **92**(6), 531–550 (2012)
28. Pierré, J.E., Passieux, J.C., Périé, J.N.: Finite element stereo digital image correlation: framework and mechanical regularization. Experimental Mechanics **53**(7), 443–456 (2017)
29. Pierré, J.E., Passieux, J.C., Périé, J.N., Bugarin, F., Robert, L.: Unstructured finite element-based digital image correlation with enhanced management of quadrature and lens distortions. Optics and Lasers in Engineering **77**, 44–53 (2016)
30. Réthoré, J.: A fully integrated noise robust strategy for the identification of constitutive laws from digital images. Int. J. Numer. Meth. Eng. **84**(6), 631–660 (2010)
31. Réthoré, J., Muhibullah, Elguedj, T., Coret, M., Chaudet, P., Combescure, A.: Robust identification of elasto-plastic constitutive law parameters from digital image using 3D kinematics. Int. J. Solids and Structures **50**, 73–85 (2013)
32. Reu, P.L., Rohe, D.P., Jacobs, L.D.: Comparison of {DIC} and {LDV} for practical vibration and modal measurements. Mechanical Systems and Signal Processing pp. – (2016)
33. Serra, J., Pierré, J.E., Passieux, J.C., Périé, J.N., Bouvet, C., Castanié, B.: Validation and modeling of aeronautical composite structures subjected to combined loadings: the vertex project. part 1: Experimental setup, fe-dic instrumentation and procedures. Composite Structures **179**, 224–244 (2017)
34. Siebert, T., Wood, R., Splitthof, K.: High speed image correlation for vibration analysis. Journal of Physics: Conference Series **181**(1), 012,064 (2009)
35. Sun, Y., Pang, J., Wong, C.K., Su, F.: Finite element formulation for a digital image correlation method. Applied Optics **44**(34), 7357–7363 (2005)
36. Sutton, M., Orteu, J.J., Schreier, H.: Image correlation for shape, motion and deformation measurements: Basic Concepts, Theory and Applications. Springer, New York, NY (USA) (2009)

37. Sutton, M., Wolters, W., Peters, W., Ranson, W., McNeill, S.: Determination of displacements using an improved digital correlation method. Image and Vision Computing **1**(3), 133–139 (1983)
38. Vanlanduit, S., Vanherzeele, J., Longo, R., Guillaume, P.: A digital image correlation method for fatigue test experiments. Optics and Lasers in Engineering **47**(34), 371 – 378 (2009)
39. Wang, W., Mottershead, J.E., Siebert, T., Pipino, A.: Frequency response functions of shape features from full-field vibration measurements using digital image correlation. Mechanical Systems and Signal Processing **28**(0), 333 – 347 (2012)
40. Warburton, J.R., Lu, G., Buss, T.M., Docx, H., Matveev, M.Y., Jones, I.A.: Digital image correlation vibrometry with low speed equipment. Experimental Mechanics **56**(7), 1219–1230 (2016)
41. Warren, C., Niezrecki, C., Avitabile, P., Pingle, P.: Comparison of FRF measurements and mode shapes determined using optically image based, laser, and accelerometer measurements. Mechanical Systems and Signal Processing **25**, 2191–2202 (2011)
42. Zou, X., Conti, M., Dez, P., Auricchio, F.: A nonintrusive proper generalized decomposition scheme with application in biomechanics. International Journal for Numerical Methods in Engineering p. online first. DOI 10.1002/nme.5610